Colloid Polym Sci 278: 1019–1031 (2000)
© Springer-Verlag 2000

ORIGINAL CONTRIBUTION

H. Fischer
R. Weidisch
M. Stamm
H. Budde
S. Höring

The phase diagram of the system poly(styrene-*block*-*n*-butyl methacrylate)

Received: 7 December 1999
Accepted: 28 April 2000

H. Fischer (✉)
TNO-TPD, Materials Division
Institute of Applied Physics
POB 595, 5600 AN Eindhoven
The Netherlands
e-mail: hfischer@tpd.tno.nl
Tel.: +31-40-2650151
Fax: +31-40-2449350

R. Weidisch · M. Stamm
Max-Planck-Institut für Polymerforschung
Postfach 3148, 55021 Mainz, Germany

H. Budde · S. Höring
Martin-Luther-Universität
Halle-Wittenberg, Institut für Technische
und Makromolekulare Chemie
06099 Halle/Saale
Germany

Abstract The morphological phase diagram of poly(styrene-*block*-*n*-butyl methacrylate), P(S-*b*-*n*-BMA), has been investigated in detail using thermal analysis, microscopy, rheology and scattering techniques. The system shows an upper critical order transition as well as a lower critical order transition (LCOT). For the first time, morphologies of the ordered system at higher temperatures (LCOT) as well as of a block copolymer system frozen-in during the phase separation process are reported. The Flory–Huggins interaction parameter, χ depends not only on temperature, but also on the composition and the molecular weight of the block copolymers, resulting in an asymmetrical phase diagram. Furthermore, the deuteration of the PS block seems to increase the χ parameter of the P[(d_8)S-*b*-*n*-BMA] system, reflecting the influence of small changes in architecture on phase behavior. The phase behavior and morphology of PS-*b*-PBMA are summarized in a phase diagram which is, however, quite complex and therefore needs further discussion. The equilibrium morphologies displayed are influenced by the temperature-dependent-conformation term as well as by the composition term.

Key words Block copolymers · Interaction parameter · LCOT · Phase diagram

Introduction

The investigation of block copolymers as an example of systems with highly ordered structures on the nanometer scale peaked for a second time in the last 10 years after the period when they became available in a highly defined manner thanks to the development of controlled sequential anionic polymerization. The morphologies displayed and the circumstances which lead to their formation are fairly well understood, and block copolymers of the systems poly(styrene-*b*-butadiene-*b*-styrene) or poly(styrene-*b*-isoprene-*b*-styrene) are widely used in industry under the trade name Kraton for many applications. However, ordering phenomena on nanoscopic dimensions are still the subject of many theoretical and experimental investigations. Since block copolymer systems generally undergo an order–disorder transition with increasing temperatures (upper critical order temperature, UCOT) only a few systems are known which display additionally or exclusively a disorder–order transition (lower critical order temperature, LCOT) at higher temperatures [1, 2]. This transition has, in principle, the same nature as the well-known lower critical solution temperatures as observed in polymer solutions and polymer blends. While the UCOT is mainly driven by enthalpic contributions, the LCOT can only be explained by the increase in the number of possible conformations with increasing temperature as a result of volume expansion. The volume expansion causes a weakening of the enthalpic interactions and can lead to phase separation. This transition therefore has a strong entropic nature. These effects are observed in cases of block copolymers such as in the poly(styrene-block-*n*-butyl methacrylate), P(S-*b*-*n*-BMA), system

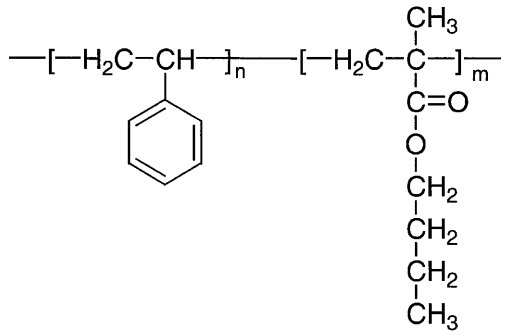

Fig. 1 Chemical structure of the poly(styrene-*block*-*n*-butyl methacrylate) [P(S-*b*-*n*-BMA)] block copolymers

(Fig. 1), where a voluminous side group can lead to the conformational volume effects at higher temperatures as described previously.

A recently published study, however, describes block copolymer systems with even more voluminous side groups having only one, an UCOT behavior [3]. This results not only from the effects described before, but also from a change in compatibility due to a number of other factors. These factors include decreasing chain flexibility and increasing self-interaction energies of the pure components as seen by the change in the value of the total solubility factor or in the calculated specific volume with increasing number of carbons in the alkyl side chains [3]. An approximation of noncompressibility of the system is no longer justified at higher temperature since the volume expansion results in an increase in free volume and availability of configurations. The phase separation is accompanied by a net increase in volume, which increases the entropy of the system; therefore, the location of the LCOT has to be pressure-dependent. This has recently been successfully verified by Pollard et al. [4]. Experimentally, the LCOT is seen to shift according to the predictions towards higher temperatures as the pressures increases. The promotion of miscibility as pressure increases is a clear sign for the entropic origin of the LCOT. Additionally, pressure may alter the statistical segment length due to trans–gauche transitions.

On the basis of first experiments, a hypothetical phase diagram of the system P[(d_8)S-*b*-*n*-BMA] showing UCOT and LCOT behavior has been introduced [1]. This phase diagram is, however, based only on experiments carried out on symmetrically composed samples. Besides the known temperature dependence and the pressure dependence of the interaction parameter, χ, as discussed earlier, the lattice cluster theory as used by Freed and Dudowicz [5] also predicts a composition and molecular-weight dependence of χ for systems like the one described; therefore, the interaction parameter should be described as in Eq. (1).

$$\chi = \chi(T, p, N, f) \quad , \tag{1}$$

with a temperature dependency as seen in Eq. (2),

$$\chi(T, N, p, f) = \frac{\chi_h(N, p, f)}{T} - \chi_\sigma(N, p, f) \quad , \tag{2}$$

with χ_σ being related to the free volume of the system. Both χ_h and χ_σ are nearly temperature independent. The composition dependence of the interaction parameter as described in Refs. [4, 6] is most likely not of negligible influence,

$$\Gamma = -\frac{1}{2}\frac{\partial^2}{\partial f^2}[f(1-f)\chi] \quad , \tag{3}$$

since the demixing at high temperatures is of entropic nature and the possible number of degrees of freedom of conformations generated at higher temperatures will be highly dependent on the content of the very voluminous monomer building blocks. Finally, the molecular-weight dependency must also be kept in mind, especially since the system described in the present study is known to have a very small χ, which is also weakly segregated at high molecular weights.

In this article a more detailed description of the phase behavior and the phase diagram of the P(S-*b*-*n*-BMA) system based on a combination of different methods is presented.

Experimental

The block copolymers were synthesized as described previously by sequential anionic polymerization [7]. The molecular weights and compositions for the P(S-*b*-*n*-BMA) diblock copolymers used for transmission electron microscopy (TEM) and thermal investigations as well as those included in the phase diagrams are given in Refs. [8, 9]. Deuterated samples (PS block deuterated), denoted as P[(d_8)S-*b*-*n*-BMA], are used for the investigation of phase behavior. The characterization of these samples is given in Refs. [10, 11]. The small X-ray contrast between the components makes it difficult to get accurate statistics during scattering experiments and an exact calculation of the interaction parameter by model fits (Leibler fits) [10]. Therefore we had to use deuterated samples for small-angle neutron scattering (SANS) experiments. Samples (films of about 1-mm thickness) for all investigations were prepared by the following procedure. A 5% solution of the block copolymers in toluene was filtered and subsequently poured into Petri dishes. After slow removal of the solvent at 25 °C (1 week) the samples were annealed for 2 days at 80 °C in a nitrogen atmosphere. This temperature does not seem to be very suitable, since the glass-transition temperature (T_g) of PS is at about 100 °C. However, results presented later indicate that an order–disorder transition occurs around 85 °C and, therefore, microphase separated morphologies can be found below this temperature. Annealing above temperatures of 85 °C could therefore induce mixing and hence prevent us from observations of phase-separated samples in the lower-temperature region. Furthermore, the morphologies in the LCOT regime were investigated after annealing samples at 150 °C and subsequent quenching to room temperature.

For thermal characterization a Perkin-Elmer DSC7 with scanning rates of 10 K/min and a Rheometrics RDA II in torsion-testing mode with a frequency of 1 Hz and a heating rate of 2 K/min were employed. TEM investigations were performed on ultramicrotomed slices of thickness between 60 and 100 nm on a

JEOL 2000 FX operating at 80 keV. The samples were inspected unstained or stained by RuO_4 vapor. Low-angle electron diffraction (LAED) experiments were performed as described earlier [12]. For the small-angle X-ray scattering (SAXS) experiments a small-angle camera on a rotating anode X-ray source equipped with a heating cell and the small angle setup on the A2 beamline (polymer beamline) at the synchrotron source Hasylab, Hamburg (Germany), were used. SANS experiments on samples with deuterated styrene blocks [11] were performed at the ILL, Grenoble, (SANS beamline) and at the GKSS, Geesthacht. The instrument configuration was $\lambda = 0.91$ nm and $\Delta\lambda/\lambda = 0.2$ (Geesthacht) or 0.1 (Grenoble) due to the velocity selector and sample–detector distance of 5.6 m. The scattering data were corrected for detector sensitivity, background scattering, sample thickness and transmission and were placed on an absolute basis using several standards. The SANS profiles at different temperatures are discussed as a function of the scattering vector, $q = (4\pi/\lambda)\sin(\theta)$, where 2θ is the scattering angle. χ parameters were calculated using Leibler fits to the scattering curves in the disordered state [10].

Rheological measurements were carried out using a Rheometrics RMS 800 with a cone–plate geometry, a cone angle of 0.1 rad and a diameter of 0.5 in. The samples were sheared between the conical gap enclosed by the cone and plate in an oscillatory mode at different temperatures. The experiments were carried out in a dry nitrogen environment.

Results and discussion

Thermal analysis

A first determination of the phase separation between the two blocks is possible by a measurement of the T_g by differential scanning calorimetry (DSC) and dynamic mechanical analysis (DMA) of the materials (Fig. 2).

Block copolymers with $M_n > 200$ kg/mol (212–400 kg/mol) generally show two T_gs, indicating a phase separation between the two blocks; however, some remarkable tendencies can be seen in Fig. 2. First, for phase separation at different compositions between the two blocks in the temperature range displayed, indicated by two T_gs, quite high molecular weights (200 kg/mol or greater) of the block copolymers are needed. This fact hints at a rather weak repulsion between the two blocks and to a very small interaction parameter, χ. Second, the phase separation tendency seems to be strongly dependent on the composition of the block copolymers. Block copolymers with asymmetric compositions ($f_{PS} > 0.6$) and a low molecular weight (around 100 kg/mol) show a clear tendency towards mixing of the blocks, indicated by the observation of a only one glass transition by DMA. Third, the glass transitions of the P*n*-BMA rich blocks are always slightly above the T_g of a P*n*-BMA homopolymer (31 °C), whereas the T_g of the PS-rich blocks is about the same as for PS homopolymers (100 °C). This indicates the existence of possibly mixed domains of P*n*-BMA blocks with PS blocks separated from blocks of pure PS. Again, this observation hints at a strong compositional dependence of the separation between the two blocks and at an asymmetric phase diagram.

While using precise thermal analysis, it should be possible not only to indicate the order–disorder transitions but also to measure the heat of fusion connected with this transition [13, 14]. The heating scan of a block copolymer of the system investigated is shown in Fig. 3.

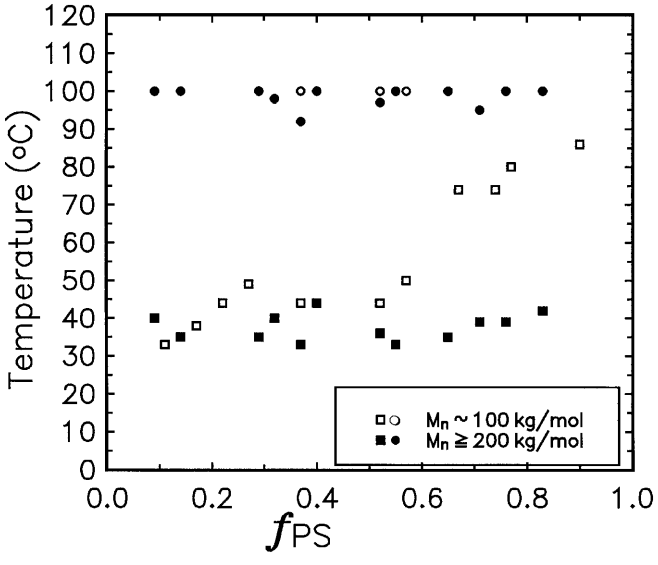

Fig. 2 Glass-transition temperatures of block copolymers of the P(S-*b*-*n*-BMA) system with respect to the composition of the block copolymers and the molecular weight. *open symbols* represent data obtained from samples with a molecular weight of approximately 100 kg/mol; *filled symbols* represent data obtained from samples with a molecular weight equal to or larger than 200 kg/mol (212–400 kg/mol)

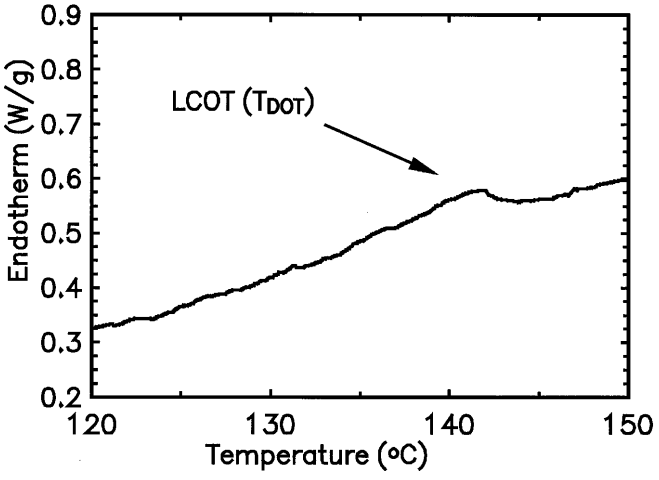

Fig. 3 Differential scanning calorimetry (*DSC*) heating scan of a sample of a P(S-*b*-*n*-BMA) diblock copolymer (molecular weight 212 kg/mol, $f_{PS} = 0.4$). The scan rate was 10 K/min. The scan shows a peak which can be associated with the lower critical order transition (*LCOT*) (disorder–order transition)

Here, a peak is found which can be associated with the LCOT (disorder–order transition) similar to the peak described earlier in the system poly(styrene-*block*-isoprene) [P(S-*b*-I)] [13] for the UCOT (order–disorder transition). The results of a more careful experiment are shown in Fig. 4.

Here, the specific heat of a sample with a molecular weight of about 212 kg/mol and a PS content of 40 vol% recorded in a heating and a cooling scan is plotted against the temperature. In both scans a significant change in slope at temperatures of about 100 °C (negative: order–disorder transition temperature; positive: disorder–order transition temperature) are seen. These phase transitions are spread over a relatively wide temperature range owing to the high molecular weight of the sample and therefore long relaxation times or diffusion times. This is also the reason why the order–disorder transition temperatures can only be estimated by DSC. Reversibility of the experiments turned out to be very difficult owing to the rather long diffusion times of the different blocks. Reproducibility, however, has been proved for several experiments using different samples.

Rheology

A more accurate determination of order–disorder transition temperatures is possible from rheological experiments. Such experiments were used by Ruzette et al. [3], Weidisch et al. [8] and Karis et al. [15] for the determination of the LCOT temperatures. These experiments, however, showed the phase transition only with rheology and good agreement using scattering techniques was not observed. A clear indication of order–order and order–disorder transitions is described in the case of the P(S-*b*-I) system by Förster et al. [16] Khandpur et al. [17] and Han et al. [18]. They also measured G' in dynamic experiments and plotted it against the temperature to identify phase transitions and to gain information about phase morphologies. A phase transition can be identified by rheological experiments where a monotonic decrease in G' is followed by a significant decrease close to the order–disorder transition temperature or by a jump indicating the build up of a newly ordered phase during a disorder–order transition. A typical plot of the results of a rheological experiment for a deuterated P[(d_8)-S-*b*-*n*-BMA] (f_{PS} = 0.55, M_n = 90 kg/mol) is shown in Fig. 5.

The plot displayed in Fig. 5 clearly shows a steady decrease in G' with temperature, followed by a jump at about 154 °C. This jump is attributed to the LCOT of the sample: the increase in G' at higher temperatures indicates an ordering process resulting in an ordered structure revealing a significantly higher shear modulus than the disordered melt. Furthermore, the shear storage modulus remains at a constant level in spite of increasing temperatures and shows no tendency of softening, which indicates the presence of a thermodynamically stable phase-separated morphology at higher temperatures. This type of experiment is reproducible while using small shear rates of 0.01 rad/s. Furthermore, it is also possible to verify the location of the LOCT by temperature-dependent scattering experiments (Fig. 6). The detection of the UCOT by means of rheology is, however, not

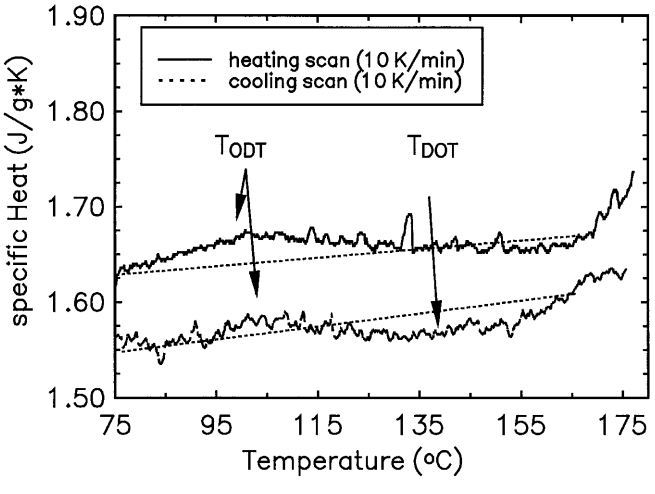

Fig. 4 Plot of the specific heat versus temperature of a P(S-*b*-*n*-BMA) diblock copolymer (molecular weight 212 kg/mol, f_{PS} = 0.4). The scan rate was 10 K/min. The *upper scan* shows one change and the *lower scan* shows two changes in the slope of the temperature dependence of the specific heat which can be associated with the upper critical order transition (*UCOT*) (order–disorder transition) and the LCOT (disorder–order transition)

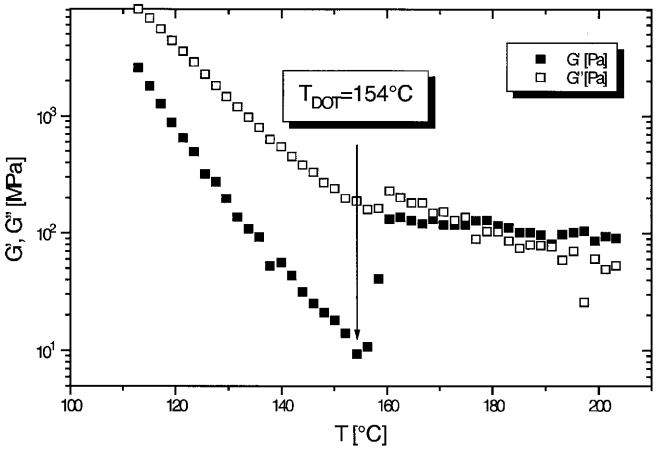

Fig. 5 Plot of G' and G'' against the temperature of a P(d_8 S-*b*-BMA) diblock copolymer with 90 kg/mol and 55% PS. The measurement was performed at ω = 0.01 rad/s; the sample was annealed before each measurement, represented by an experimental point, for 20 min. A disorder–order transition temperature (LCOT) can be observed

possible due to the glassy state of the PS block at these temperatures.

SAXS and SANS

Temperature-dependent SAXS and SANS experiments similar to those described earlier [1] confirmed the existence of an order–disorder (UCOT) and a disorder–order transition (LCOT, Figs. 6–8) under heating conditions.

A sample with a molecular weight of 148 kg/mol and a PS content of 25% shows a order–disorder transition at about 75–80 °C upon heating (Fig. 7).

Temperature scans upon heating a block copolymer sample with a molecular weight of 130 kg/mol and a PS content of 47 vol% are shown in Fig. 8. Here, the UCOT takes place between 100 and 110 °C and LCOT at about 180 °C. This sample has about the same composition as the samples of the deuterated block copolymers described in Ref. [1]; however, for the P(S-*b*-*n*-BMA) system the temperature range for the disordered phase seems to be larger than suggested by the previous experiments on deuterated samples of P[(d_8)-S-*b*-*n*-BMA] by Russell et al. [1]. The differences in behavior between the present system and the deuterated system seem to be relevant in contrast to the discussions in the literature owing to the weakly segregated phases in our system, which has particularly small values of the interaction parameter. The influence is not as pronounced for systems such as poly(styrene-*block*-butadiene) (strong segregation limit).

The dependence of the slope of the scattering vector on temperature for the same sample as used in the rheological experiment shown in Fig. 5 is illustrated in Fig. 6. As shown by Rosedale et al. [19] the slopes of the plots of the scattering vector are different for the ordered and disordered phases according to the deviation of the chain conformation from the Gaussian coil in the ordered phase.

A change in slope located at about 155 °C has been observed [14], confirming the general results of Rosedale et al. in this case for LCOT behavior. This temperature

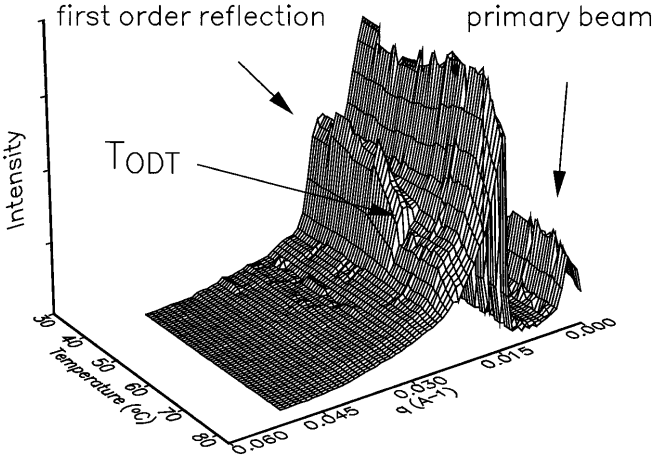

Fig. 7 3D small-angle X-ray scattering (*SAXS*) plot of the small-angle diffraction pattern of a sample of a block copolymer of the P(S-*b*-*n*-BMA) system (molecular weight 148 kg/mol, f_{PS} = 0.25) during heating. The scans were obtained in temperature steps of 5 K with a time between the scans of about 30 min. The collection time for one scan was 2 min. An order–disorder transition temperature (UCOT) can be observed upon heating; this transition cannot however, be found upon cooling, possibly owing to very long diffusion times and a slow diffusion below the glass-transtion temperature of the PS blocks

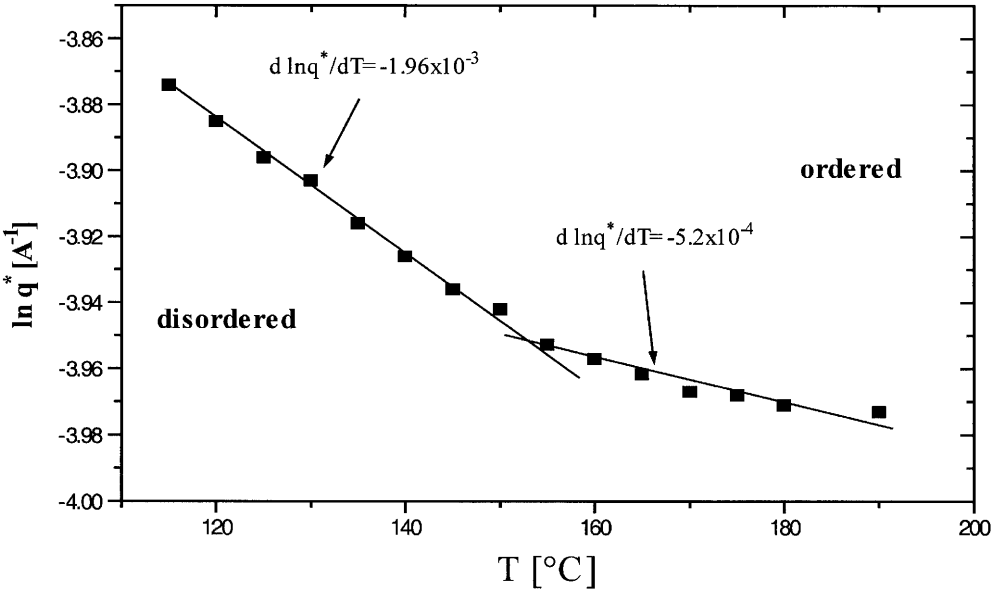

Fig. 6 Plot of the temperature dependence of the scattering vector of one sample of the P[(d_8)S-*b*-*n*-BMA] system (molecular weight 90 kg/mol, f_{PS} = 0.55, same sample as in Fig. 5). A change in the slope indicates the disorder–order transition upon temperature increase

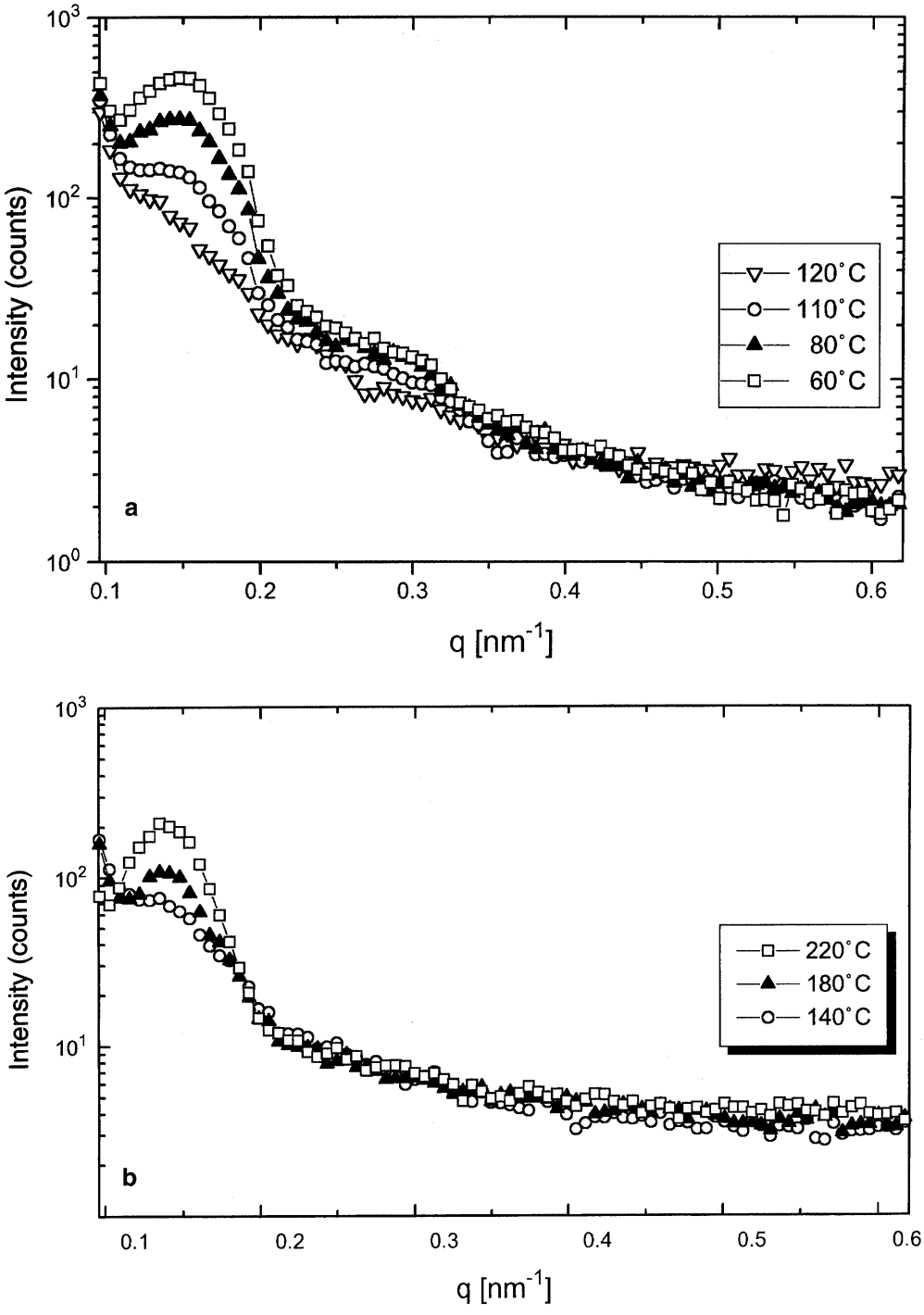

Fig. 8a, b 2D SAXS plots of the small-angle diffraction pattern of a sample of a block copolymer of the P(S-*b*-*n*-BMA) system (molecular weight 123 kg/mol, $f_{PS} = 0.47$) during heating. The scans were obtained at discrete temperatures as indicated in the plots; the time between the different experiments was about 30 min. The collection time for one scan was about 2 h. An order–disorder transition temperature (UCOT) upon heating and the LCOT (disorder–order transition) can be observed. The UCST must be located between 110 and 120 °C, the LCOT around 140 °C. Since the interval between the discrete experiments is too large to determine the UCOT and the LCOT precisely, a numerical value for both has not been given

can thus be attributed to the disorder–order transition (LCOT). The value is in good accordance with values obtained in our rheological experiments as described earlier. Furthermore, we recently showed [10] that the peak intensity, $I(q^*)$, and the full width at half-maximum, Δq, as a function of temperature strongly increased at 155 °C, indicating a disorder–order transition (LCOT) at this temperature.

The phase diagram for the UCOT regime

The morphological phase diagram for the UCOT behavior of the system discussed shows the existence of different morphologies with respect to molecular weight and composition. The phase diagram is constructed on the basis of our DSC, DMA and TEM investigations (Fig. 9).

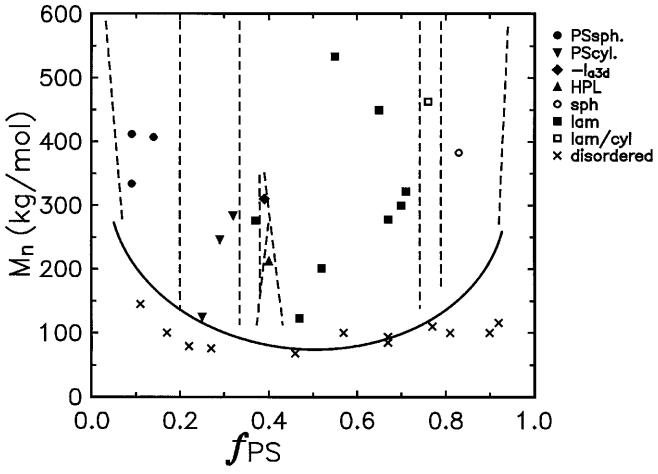

Fig. 9 Morphological phase diagram of the P(S-*b*-*n*-BMA) system as revealed by transmission electron microscopy (*TEM*). The *dashed lines* separate areas of different morphologies from each other. The abbreviations have the following meaning: PS_{sph} = PS spheres in a P*n*-BMA rich matrix, PS_{cyL} = PS cylinders in a P*n*-BMA rich matrix, *-Ia3d* = gyroid structure, *HPL* = hexagonal perforated lamellae of PS, *lam* = lamellae of PS and P*n*-BMA rich material, *lam/cyl* = coexistence of lamellae and cylinders of P*n*-BMA rich material in PS, *sph* = P*n*-BMA rich material in a PS matrix, *disordered* = mixed phase. The *line* is a guide for the eye

The phase diagram shows all principal morphologies as known from other systems as well as the gyroid phase and hexagonally perforated lamellae [16, 20] (Fig. 10).

A detailed description of the discrimination between the several cubic phases in block copolymers is described in Ref. [21]. Here we see in the TEM picture a threefold symmetry in the connection points hinting to the space group *-Ia3d*. Furthermore, the indexing of the LAED pattern allows the gyroid phase to be identified with confidence.

However, as discussed earlier [8, 10], the general appearance is highly asymmetric. Furthermore, the diversity of morphologies is less rich at high PS contents. Morphologies such as gyroid or hexagonally perforated structures are not observed in our experiments in the PS-rich region of the phase diagram and lamellae and cylinders coexist instead [8]. This structure is most probably a nonequilibrium structure resulting from a very small χN and hence a very small driving force for microphase separation owing to a small diffusion coefficient connected to samples having high molecular weights. This region appears at the PS-rich side of the phase diagram ($0.74 < f_{PS} < 0.79$). A calculation based on the free energy of the system represented as the sum

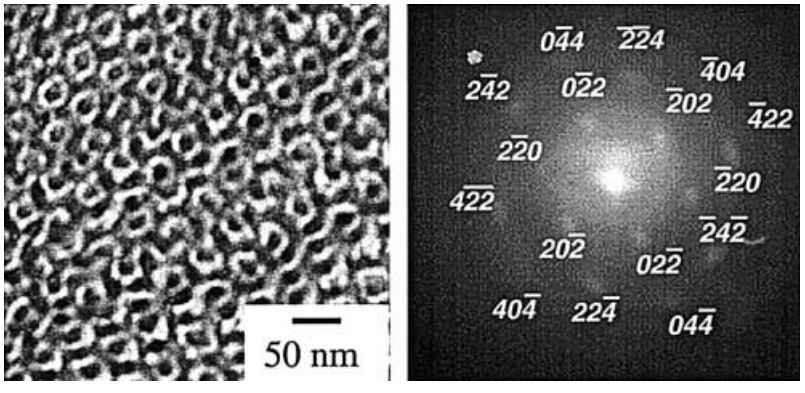

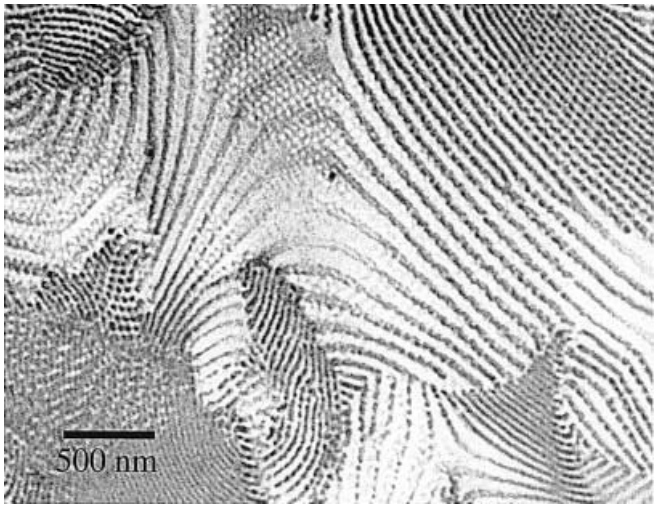

Fig. 10 a TEM micrograph of a sample of the P(S-*b*-*n*-BMA) system (molecular weight 270 kg/mol, $f_{PS} = 0.39$, $T = 25$ °C). The sample shown was not stained: a natural contrast appeared after a short exposure to the electron beam. The picture shows a *-Ia3d* or gyroid structure, together with a low-angle electron diffraction pattern obtained from the same sample using a virtual camera length of 10 m [12]. **b** TEM micrograph of a sample of the P(S-*b*-*n*-BMA) system (molecular weight 212 kg/mol, $f_{PS} = 0.40$, $T = 25$ °C). The sample shown was not stained: a natural contrast appeared after a short exposure to the electron beam. The picture shows an HPL structure

of the elastic energy and the interface energy contributions, where the segment length and the molecular volumes of the monomeric units are used as parameters, supports our experimental results for transitions between different morphologies with respect to the block copolymer composition in the phase diagram [22].

The existence of the demixed phase at lower temperatures (below the UCOT) has been discussed only as a consequence of a phase separation using solvents; however, the reported morphologies are found in annealed samples (at 80 °C); thus, an instable system should be mixed with a homogeneous system. Furthermore, a ternary system of a blend dissolved in a solvent tetrahydrofuran (THF) clearly shows phase separation behavior at lower temperatures [23]. Stable phase separation below the T_g of PS has been reported for the deuterated system by Russell et al. [1] This confirms our observation of microphase separated morphologies below the T_g of PS and the existence of a UCOT for P(S-*b*-*n*-PBMA).

The reversibility of the UCOT seems to be particularly difficult since the UCOT takes place at approximately 80 °C, which is below the T_g of PS. Furthermore, the high molecular weights (above 100 kg/mol) also make phase separation very difficult, at least to reach an equilibrium morphology during the cooling process because the diffusion times are expected to be rather large. In addition, the driving force is very small since the interaction parameter is very small and the system is clearly in the weak segregation limit. Therefore, until now the morphologies displayed by the solvent-prepared samples can be seen as a representation of stable phase separation below the UCOT [1, 8, 24, 25].

An interesting picture is shown in Fig. 11. Here, a TEM image of a symmetrical block copolymer sample with a molecular weight of about 85 kg/mol is shown. The picture displays the growth of an ordered domain (lamellar morphology) in a disordered matrix and frozen-in during phase separation. The phase boundary appears to be very sharp, indicating a first order transition; however, if one looks more closely in the matrix material, darker and lighter domains become visible. This effect is enhanced by the staining procedure. The darker and lighter areas represent areas of different electron densities and, hence, of different bulk densities. Most likely, we have here a visualization of density fluctuations in the disordered phase. The dimensions of the fluctuations are of the order of a few tens of nanometers as shown in the TEM micrograph in Fig. 11.

An equation describing the temperature dependency of χ in the whole temperature range (UCOT and LCOT) is not available from our experiments. For high temperatures, data from SANS experiments can be used, as discussed later; however, for temperatures below the UCOT the temperature dependence of χ based on results from SANS experiments is not available. Therefore, for the discussion of phase behavior below the UCOT ($T < 80$ °C) we use the data describing the composition dependence of χ rather than the temperature dependence, which will be used in the following discussion.

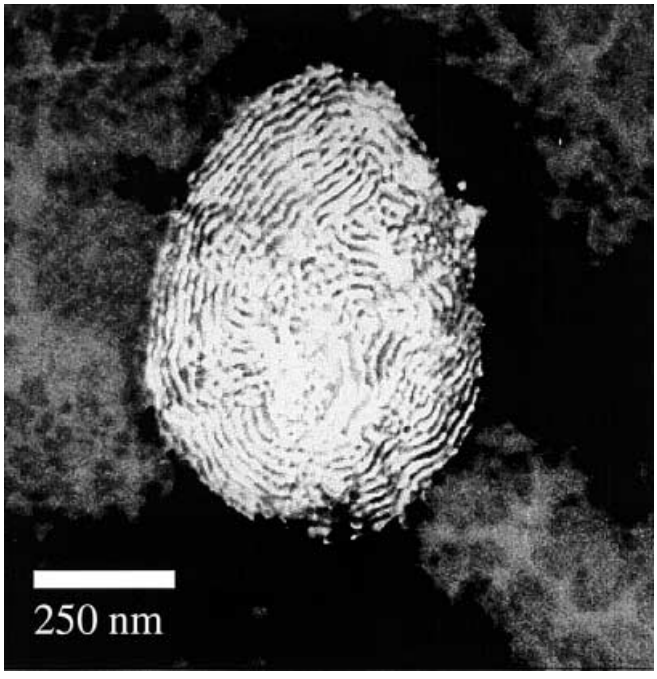

Fig. 11 TEM micrograph of a sample of the P(S-*b*-*n*-BMA) system (molecular weight 85 kg/mol, $f_{PS} = 0.67$, $T = 25$ °C). The sample shown was stained to enhance the natural contrast. The picture shows one of the islands of phase-separated material (lamellar morphology) surrounded by mixed material of the sample. The *dark* and *light* areas represent areas of different electron densities as a result of different concentrations of PS and PBMA. Most likely, this represents a visualization of density fluctuations in the disordered phase

The transformation of the data into a morphological phase diagram demonstrating the existence of different morphologies with respect to composition and χN is quite complex because $\chi_{P(S\text{-}b\text{-}n\text{-}BMA)}$ corresponds either to a temperature dependence above 100 °C (SANS) [10, 24] or to a composition dependence at room temperature [23]. A numerical description of χ in the complete temperature range for the UCOT and LCOT regions is not available; however, from our thermal and microscopic analysis it is already understood that the value of χ must be very small.

The interaction parameter in the UCOT region

Geveke and Danner [23] published data for the composition dependence of the interaction parameter $\chi_{(PS\text{-}Pn\text{-}BMA)}$ for blends. These measurements were performed at 30 °C in THF and show substantial asymme-

try of the mixing/demixing behavior. The concentration dependence of the interaction parameter can be described by a simple equation

$$\chi = \chi_a + \chi_b \frac{f_{Pn\text{-BMA}}}{f_{PS} + f_{Pn\text{-BMA}}} \quad . \tag{4}$$

The values for χ_a and χ_b are 0.0128 and −0.00733 as given by Geveke and Danner. This dependency seems to be important for the PS-*n*-BMA system, where a strong compositional dependence of χ, on the basis of increments obtained from a liquid–liquid phase equilibrium method and also from experiments, has been described [26]. This calculations show a linear dependence of χ on polymer concentration as expressed in Eq. (4). This dependence is attributed to the difference in monomer volumes of the blocks, which is the case for P(S-*b*-*n*-PBMA), as described by Koningsveld et al. [27] for polymer blends.

On the basis of calculations by Geveke and Danner we are able to construct a morphological phase diagram for a temperature of 30 °C similar to that published by Bates et al. [20] for the systems P(S-*b*-I) and poly(ethene-*block*-ethylethene). However, in our case the phase diagram is constructed only by a variation of N and f only and not by a variation of N, f and T.

The phase diagram in Fig. 12 clearly shows the asymmetry already discussed. On the basis of the difference in monomer volumes as well as the segment length for P(S-*b*-*n*-BMA) the composition dependence of χ has to be discussed. This difference is also the reason for the observed asymmetry of the phase diagram shown in Fig. 12. The asymmetric phase diagram is supported

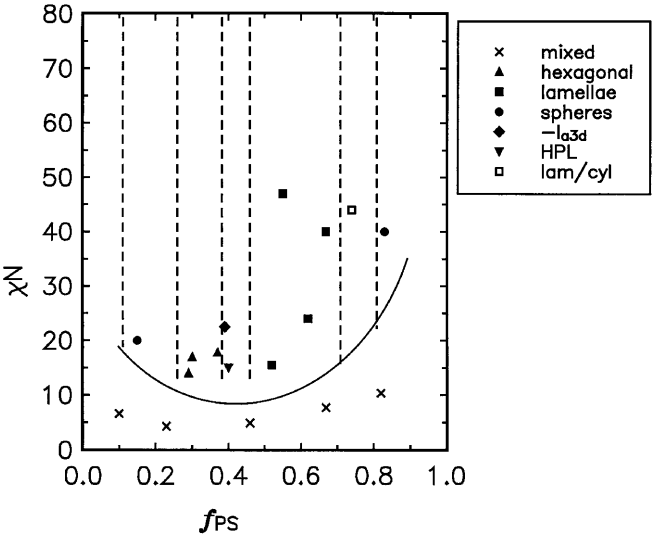

Fig. 12 Morphological phase diagram of the P(S-*b*-*n*-BMA) system with respect to the composition of the block copolymer and the χN value. The *dashed lines* separate areas of different morphologies from each other. The abbreviations have the same meaning as in Fig. 9

by the calculation of the morphologies based on a model of Alexander and DeGennes used by Sehubert et al. [24] for ABC triblock copolymers. It is shown that transitions for lamellar and hexagonal morphologies do not occur at the same compositions on both sides of the phase diagram.

The interaction parameter in the LCOT region

Recently, it was discussed that the present system shows both UCOT and LCOT behavior at higher temperatures [1, 3, 10]. Schubert et al. [24] published earlier values for the interaction parameter of the deuterated system P(*d*)S/P*n*-BMA (blends) using neutron reflectometry; however, their data were only obtained in a temperature range between 100 and 150 °C. These data indicate a tendency for a blend system to mix at higher temperatures (UCST). However, if our block copolymer system shows an LCOT at these temperatures [1, 25], the values for the interaction parameter of Schubert et al. [24] cannot be used for the description of the phase behavior at these temperatures. More recent experiments on samples of block copolymers of this system with deuterated PS blocks provide exact values for the interaction parameter, which increases with increasing temperature. These data are well in accordance with the prediction and observation of the LCOT behavior at higher temperatures [1, 3, 4, 10, 25]; therefore, in the present study the temperature dependence of χ reported by Weidisch et al. [10] on the basis of SANS experiments at $T > 100$ °C is used, where χ increases with increasing temperature as discussed in Ref. [10] Usually, one assumes that χ shows a linear dependence on temperature, represented by Eq. (5), which is also valid for our system:

$$\chi = \chi_H + \chi_S T \quad . \tag{5}$$

However, the investigation of P[(d_8)S-*b*-*n*-BMA] with asymmetric compositions has shown [11] that χ also depends on composition. A plot of the temperature dependence of χ for different compositions is shown in Fig. 13 and Fig. 14 shows the composition dependence of the χ_H and χ_S terms of Eq. (5), representing the entropic (χ_H) and enthalpic contributions (χ_S) to χ. The temperature dependence of the interaction parameter is very small for symmetric compositions and increases with increasing asymmetry of the composition. Furthermore, a dependence of χ on molecular weight is found as shown in Fig. 15.

The mean-field theory, which is based on equal Kuhn segment lengths and monomer volumes of the corresponding homopolymers, cannot explain the composition dependence of the χ parameter. However, for P(S-*b*-*n*-BMA) diblock copolymers the segment length as well the monomer volumes of the corresponding

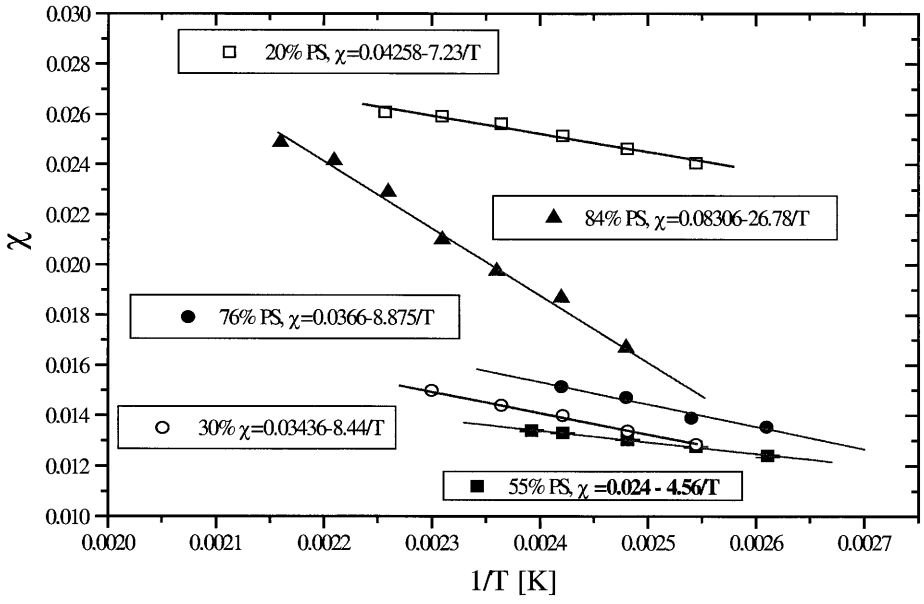

Fig. 13 Plot of the temperature dependence of the interaction parameter for samples with different compositions for the P[(d_8)S-*b*-*n*-BMA] system (molecular weight of the samples 90–130 kg/mol, f and T variable). The temperature dependence of the interaction parameter increases with increasing asymmetry of the block copolymers

blocks are different. For polymer blends, the composition dependence of χ is given by the theory of Freed and Dudowitz. Furthermore, the dependence of χ on molecular weight is also included in the lattice cluster model of Dudowitz and Freed [28] for polymer blends.

A parabolic dependence of χ on composition has already been described for poly(ethyl ethylene)/poly (vinyl methyl ether) blends [29].

The theory of Dudowitz and Freed [28] predicts a decrease in the interaction parameter with increasing molecular weight; this is also found in our system (Fig. 15).

The final phase diagram

Finally, it is possible to construct a T–f phase diagram of the system including data obtained from our experiments (Fig. 16). It is shown that for P(S-*b*-*n*-BMA) diblock copolymers the interaction parameter depends on composition as well as on molecular weight and the phase behavior appears to be quite complex. Furthermore, the existence of a UCOT and an LCOT for this system complicates a detailed discussion of the phase diagram; therefore, the χN–f phase diagram cannot be presented in this study and further investigations are necessary to calculate $(\chi N)_{crit}$ values for different compositions and molecular weights.

The phase diagram displayed is again asymmetrical as described previously. Furthermore, only a small molecular-weight dependence of the UCOT is found compared to the LCOT. That could be attributed to the fact that the order-disorder-transition (ODT) exists below the T_g of the PS block; therefore, it is difficult to reach the UCOT while cooling from high temperatures. The dynamics of the system is confined and an equilibrium cannot be reached and the reversibility of the UCOT transition is very difficult to observe. A similar observation with respect to the reversibility and the problems of its detection for the system described has been mentioned by Russell et al. [1]. Our results confirm the UCOT behavior observed by Russell and coworkers using SAXS. The UCOT is not reversible owing to the proximity of the T_g and the UCOT, which is associated with very long relaxation times near the T_g of PS.

The differences in chemical nature, chemical potential and chain structure of PS and PBMA lead to noncompatibility, which has even been found in binary solutions in CCl_4, where the system exists only in two phases, a PS-rich phase and a PBMA-rich phase (both about 70–80% of the respective polymer component) [30]. The use of a supercritical solvent such as CO_2, as described recently by Watkins et al. [31] does not influence the general tendency of phase separation but lowers the LCOT transition temperatures. It is, however, not applicable for lowering the UCOT temperatures since the CO_2 dilutes selectively the P*n*-BMA blocks. This explains why microphase separated morphologies can be expected at lower temperatures (T < 80 °C) using solvent cast samples.

Above the LCOT it was possible to quench the samples rapidly to room temperature and to inspect their morphology. This is the first time that morphologies in the upper range of a phase diagram (LCOT) have been explored. The equilibrium morphologies are, however, not new. In principle the same morphologies as known for block copolymers systems revealing UCOT behavior have been observed. This is indicated

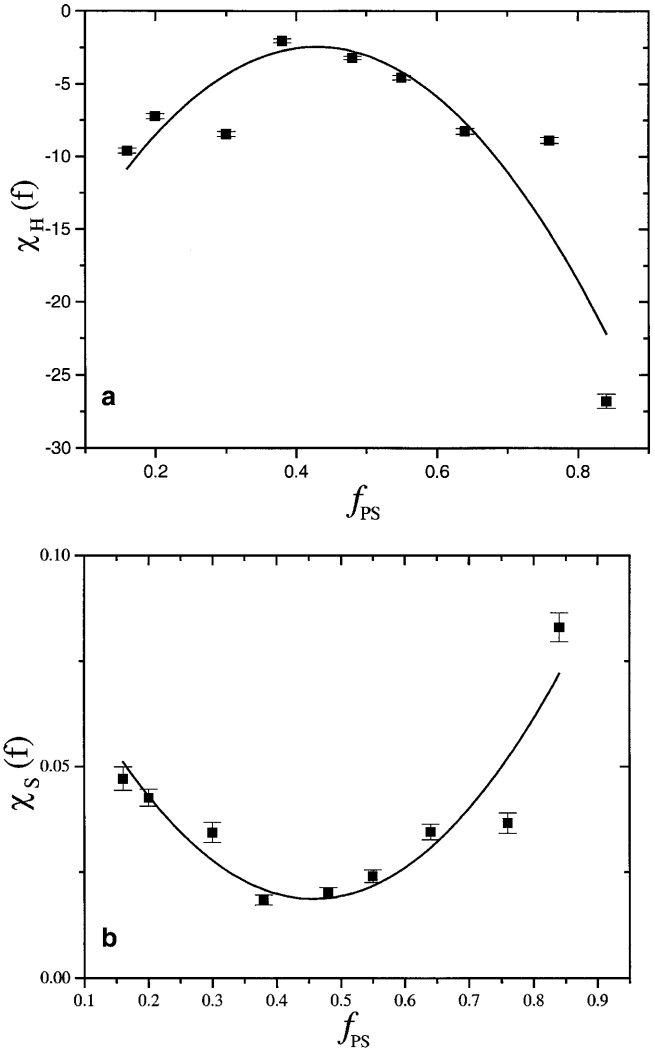

Fig. 14a, b Plot of the composition dependences of the χ_H and χ_S parameters for samples with different compositions for the P[(d_8)S-*b*-*n*-BMA] system (T = 150 °C, f variable) describing a linear temperature dependence of the interaction parameter. The *line* is a fit to the data

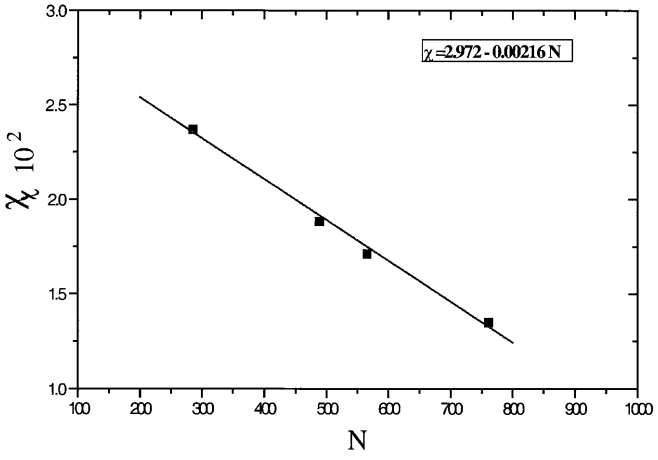

Fig. 15 Molecular weight dependence of the interaction parameter of the P[(d_8)S-*b*-*n*-BMA) system (T = 150 °C, f~0.5). The *line* is a fit to the data

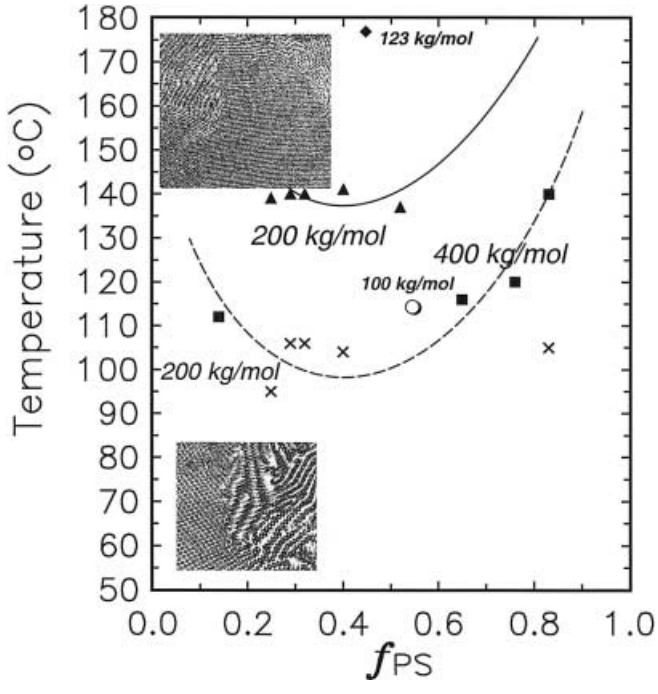

Fig. 16 Phase diagram of the P(S-*b*-*n*-BMA) system with UCOT and LCOT lines for a molecular weight of about 100, 200 and 400 kg/mol. The *symbols* represent experimental points with the following meanings: x = UCOT of samples with a molecular weight of about 200 kg/mol (DSC, SAXS), both of the symbols indicate a UCOT which, however, can only be found upon heating; ■ = LCOT of samples with a molecular weight of about 400 kg/mol (DSC), ▲ = LCOT of samples with a molecular weight of about 200 kg/mol (DSC, rheology). The datum for the deuterated sample (○; 100 kg/mol, LCOT) was taken from Ref. [1]. and that of the protonated sample (◆, 123 kg/mol, LCOT) was obtained from Fig. 9. The *inserts* represent typical morphologies (PS cylinders in a PBMA-rich matrix) as found in the demixed phase at lower temperatures (UCOT, M_n = 130 kg/mol, f_{PS} = 0.25, T = 160 °C) as well as in the demixed phase at higher temperatures (LCOT, M_n = 246 kg/mol, f_{PS} = 0.29, T = 25 °C)

for one sample shown in Fig. 16 displaying a hexagonally ordered cylinder phase.

Conclusions

The P(S-*b*-*n*-BMA) system has been analyzed with respect to its phase behavior and phase morphology. The morphologies displayed are as rich as those described for other systems [20, 32]. The UCOT and LCOT were observed for most of the samples; however, a few important findings verify the previous experiments. First, due to the small interaction parameter between PS and P*n*-BMA most of the samples are only in the weak segregation limit, leading to the separation

of a mainly pure PS phase and a mixed PS/PBMA phase associated with a relatively broad interface width [10, 33]. Second, since χ is very small, the segment architecture has a large influence on the phase behavior, and the dependence of χ on composition as well as the molecular-weight dependence cannot be neglected as clearly shown in our SANS experiments. Both lead to asymmetry of the phase diagram with respect to the composition and morphology as revealed for the UCOT detected only upon heating as well as for the LCOT.

If the segment architecture has a pronounced influence on the phase behavior, small changes such as deuteration could also influence the phase transition temperatures. The small labeled symbols in the phase diagram displayed in Fig. 16 represent data obtained from a deuterated and a protonated sample. These data differ substantially in position from each other. This indicates the better miscibility of the protonated materials with each other compared to the system with deuterated PS. The difference between the protonated and the deuterated samples could be attributed to the architectural change in the PS segments and also to changes in polarity and chemical nature. This difference can only be detected in weakly segregated systems as described in the present study.

We are only on the way to understanding the fundamental properties and behavior of polymers and block copolymers. The system described is only one of the systems which has recently gained very much attention. Here, we discussed a part of the complex miscibility and phase separation of polymer–polymer systems including asymmetry derived from the different nature of nearly compatible polymers, segments or monomers. To describe the phase behavior below the UCOT ($T < 80$ °C) the composition dependence of χ based on the work of Geveke and Danner [23] is used. For the phase behavior at high temperatures ($T > 100$ °C) more exact data based on the results of SANS experiments are available, which demonstrate the complex phase behavior of P(S-*b*-*n*-BMA) diblock copolymers concerning the dependence of χ on composition and molecular weight.

Other investigations are focused not only on the temperature dependence of phase transitions, but also on their pressure dependence behavior and on the influence of small changes in the chemical nature of the building blocks [4, 31]. The phase diagram discussed here combines results obtained by different experimental methods and explains differences to more explored, strongly segregated (concerning the χ parameter) systems. However, a complete theoretical and numerical description of the interaction parameter of the components in our system cannot be given at this time.

Acknowledgments We thank A. Meyer from the A2 beamline, Hasylab, and R. Gehrke, Hasylab, Hamburg, for support during the SAXS experiments for the determination of the T_{ODT}s. Furthermore, we would like to express our thanks to G. Höhne, University of Ulm, for the very careful thermal analysis of the LCOT and UCOT temperatures. R. W. acknowledges postdoctoral support from the Deutsche Forschungsgemeinschaft and discussions with V. Abetz (Bayreuth). We also acknowledge the help of P. Staron and D. W. Schubert during the SANS experiments at the GKSS, Geesthacht.

References

1. Russell TP, Karis TE, Gallot Y, Mayes AM (1994) Nature 368:729
2. Hashimoto T, Hasegawa H, Katayama H, Kamigato M, Sawamoto M, Imai M (1997) Macromolecules 30:6819
3. Ruzette AVG, Banerjee P, Mayes AM, Pollard M, Russell TP, Jerome R, Slawecki T, Hjelm R, Thiyagarajan P (1998) Macromolecules 31:8509
4. Pollard M, Russell TP, Ruzette AV, Mayes AM, Gallot Y (1998) Macromolecules 31:6493
5. Freed KF, Dudowicz J (1992) J Chem Phys 97:2105
6. Janssen S, Schwahn D, Mortensen K, Springer T (1993) Macromolecules 26:5587
7. Arnold M, Hofmann S, Weidisch R, Michler GH, Neubauer A, Poser S (1998) Macromol Chem Phys 199:31
8. Weidisch R, Stamm M, Michler GH, Fischer H, Jerome R (1999) Macromolecules 32:742
9. Weidisch R, Michler GH, Arnold M (2000) Polymer 42:2231
10. Weidisch R, Stamm M, Schubert DW, Arnold M, Budde H, Höring S (1999) Macromolecules, 32:3405
11. Weidisch R, Schreyeck G, Enßlen M, Michler GH, Stamm M, Schubert DW, Budde H, Höring S, Arnold M, Jerome G, Macromolecules (in press)
12. Fischer H (1992) Polymer 35:3768
13. Stühn BJ (1992) Polym Sci Polym Phys 30:1013
14. Kasten H, Stühn B (1995) Macromolecules 28:4777
15. Karis TE, Russell TP, Gallot Y, Mayes AM (1995) Macromolecules 28:1129
16. Förster S, Khandpur AK, Zhao JZ, Bates FE, Hamley IW, Ryan AJ, Bras W (1994) Macromolecules 27:6922
17. Khandpur AK, Förster S, Bates FE, Hamley IW, Ryan AJ, Bras W, Almdal K, Mortenson K (1995) Macromolecules 28:8796
18. Han CD, Baek DM, Kim JK, Ogawa T, Sakamoto N, Hashimoto T (1995) Macromolecules 28:5043
19. Rosedale JH, Bates FS, Almdal K, Mortensen K, Wignall G (1995) Macromolecules 18:1429
20. Bates FS, Schultz MF, Khandpur AK, Förster S, Rosedale J, Almdal K, Mortenson K (1994) Faraday Discuss 98:8796
21. Haiduk DA, Harper PE, Gruner SM, Honke CC, Kim G, Thomas EL, Fetters LJ (1994) Macromolecules 27:4063
22. Abetz V, Stadler R (1996) Polym Bull 37:135
23. Geveke DJ, Danner RPJ (1993) Appl Polym Sci 47:565
24. Schubert DW, Abetz V, Stamm M, Hack T, Siol W (1995) Macromolecules 28:2519
25. Hammouda B, Bauer BJ, Russell TP (1994) Macromolecules 27:2357

26. Durant YG, Sundberg DC, Guillot (1994) J Appl Polym Sci 52:1823
27. Koningsveld B, Kleintjents LA, Leblans-Vinck AM (1987) J Chem Phys 91:6423
28. Dudowicz J, Freed KF (1993) Macromolecules 26:213
29. Bates FS, Muthukumar M, Wignall GD, Fetters LJ (1988) J Chem Phys 89:535
30. Lipatov Y, Chornaya V, Todosijchuk T (1997) Colloid Interface Sci 188:32
31. Watkins JJ, Brown GD, Pollard MA, Ramachandra Rao V, Russell TP (1998) Polym Prepr Am Chem Soc Div Polym Chem 368:386
32. Leibler L (1980) Macromolecules 13:1602
33. Schubert DW, Weidisch R, Stamm M, Michler GH (1998) Macromolecules 31:3743